Vol. 24 • No. 13 • April 2 • 2014

www.afm-journal.de

ADVANCED FUNCTIONAL MATERIALS

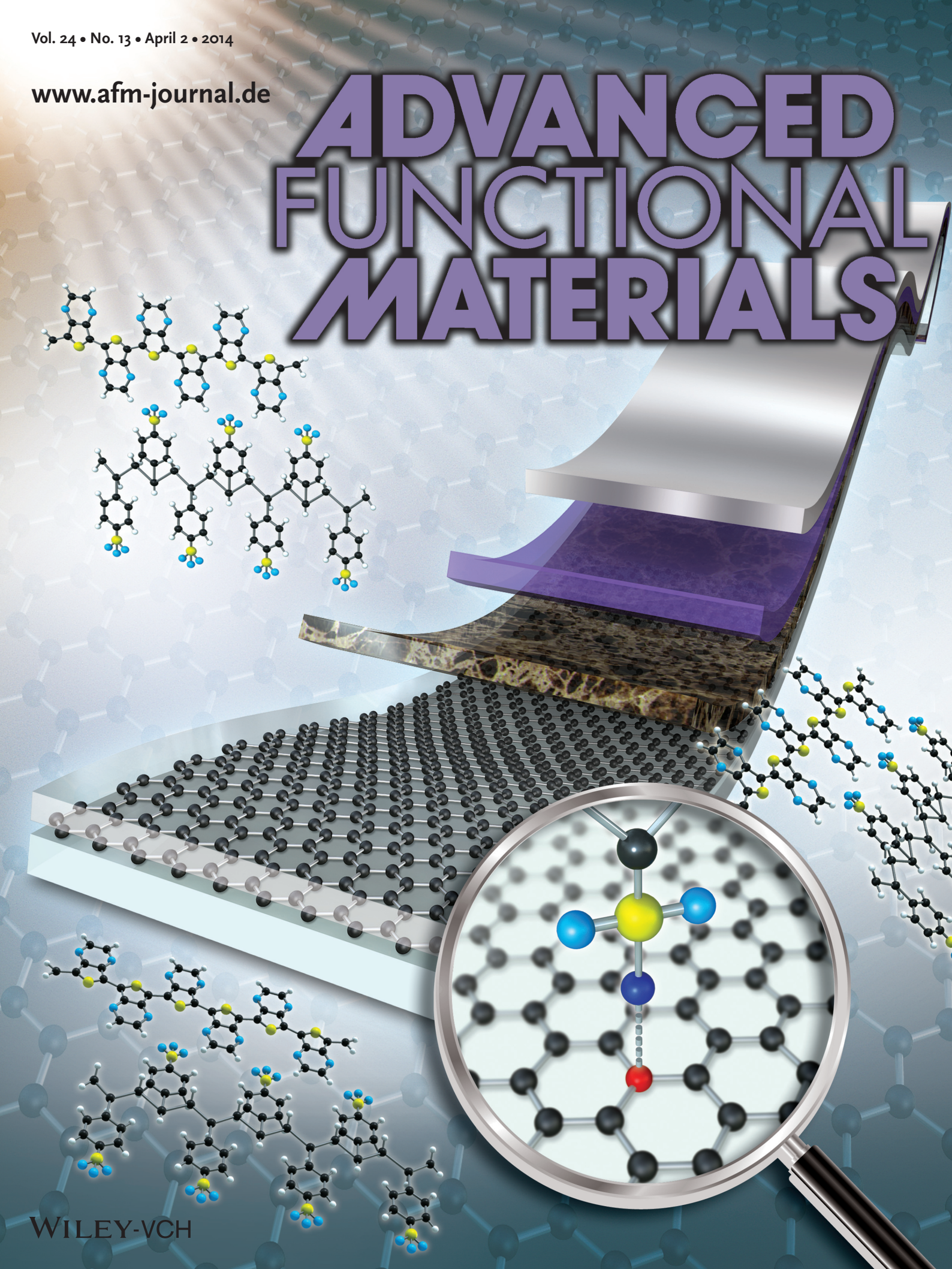

WILEY-VCH

Graphene-Conducting Polymer Hybrid Transparent Electrodes for Efficient Organic Optoelectronic Devices

Byoung Hoon Lee, Jong-Hoon Lee, Yung Ho Kahng, Nara Kim, Yong Jae Kim, Jongjin Lee, Takhee Lee, and Kwanghee Lee**

To achieve the broad utilization of the full functionality of graphene (GR) in devices, a transfer method should be developed that can simplify the process without leaving residue of the insulating supporting layer on the surface of GR. Furthermore, stable GR doping without the use of an insulating polymer is required. Here, a new GR transfer method that uses a popular conducting polymer, poly(3,4-ethylenedioxythiophene):poly(styrenesulfonate) (PEDOT:PSS), is reported as a new supporting layer for the transfer of GR films that are synthesized by chemical vapor deposition. The GR/PEDOT:PSS bilayer can be directly utilized without the removal process. Therefore, this transfer method simplifies the transfer process and solves the residue problem of conventional transfer methods. The stable doping of GR films is simultaneously achieved by using the PEDOT:PSS layer. The new GR/PEDOT:PSS hybrid electrodes are fully functional in polymer solar cells and polymer light-emitting diodes, outperforming the conventionally transferred GR electrodes and indium tin oxide electrodes.

1. Introduction

The breakthrough discovery of fabricating graphene (GR) flakes via mechanical exfoliation in 2004 began the experimental discovery of the outstanding physical and chemical properties of GR.[1] Consequently, GR was envisioned as a highly functioning component for various applications, including flexible and transparent electrodes of organic devices.[2,3] However, three key issues—high-quality synthesis, residue-free transfer, and stable doping—need to be addressed for the practical application of GR.[4–6] Although the synthesis of large-area GR via chemical vapor deposition (CVD) set a milestone in the development of GR for applications,[4,7] the latter two issues have not yet been fully satisfied. For example, despite recent progress in the use of the CVD method for the synthesis of high-quality GR sheets,[4,8] a lack of proper transfer methods that preserves their superior properties resulted in poorly performing GR electrodes in the applied organic solar cells, with a power conversion efficiency (PCE) of barely exceeding 3% value.[9–13] Although such low PCE values are also due to the use of low-efficiency photoactive materials, these values are quite low compared with devices using a conventional indium tin oxide (ITO) electrode.

The problem of conventional GR transfer mostly arises from the use of the supporting layers, which are typically composed of an insulating polymer, such as poly(methyl methacrylate) (PMMA) or thermal release tape.[4,7] They complicate the GR transfer by increasing the number of processing steps (see **Figure 1**a). The removal of the supporting layer using a reactive solvent or heat must be included to make electrical contact with the GR, which can also prohibit the use of delicate substrates such as flexible polymer substrates. Importantly, thorough-removal of the supporting layers has been found difficult.[14] The residues significantly contaminate the surface preventing good electrical contact with the GR (see Figure 1a). Therefore, a GR transfer method that uses simplified processes and does not suffer from the residue problem and the harsh removal process should be devised for the broad and full utilization of the GR's high functionality in various target devices.

Recently, intense research efforts have been implemented to overcome the transfer issue of GR. These efforts can be categorized into four major directions: 1) the direct growth of GR on dielectric substrates to eliminate the transfer process,[15] 2) the direct transfer methods that attach GR to the target substrate directly with a help of chemical glues applied to the surfaces of the targets,[16] 3) the improved cleaning methods to thoroughly remove the residues such as heating to 250–500 °C,[12,14] plasma cleaning,[17] or using stronger and/or mixed solvents,[18] and 4) the application of new supporting layers for easy removal[19] or the induction of the doping effect on GR to increase its electrical conductivity.[20,21] However, none of the reported improvements fully satisfy the need for a new transfer method for the broad and full utilization of the GR's high functionality. The approaches in the first category use high-temperature growth conditions that prohibit the use of delicate substrates. Those

Dr. B. H. Lee, J.-H. Lee, Dr. Y. H. Kahng, N. Kim, Y. J. Kim, Dr. J. Lee, Prof. K. Lee
School of Materials Science and Engineering
Heeger Center for Advanced Materials
Research Institute for Solar and Sustainable Energies
Gwangju Institute of Science and Technology
Gwangju, 500–712, Korea
E-mail: yhkahng@gist.ac.kr; klee@gist.ac.kr
Prof. T. Lee
Department of Physics and Astronomy
Seoul National University
Seoul, 151–747, Korea

DOI: 10.1002/adfm.201302928

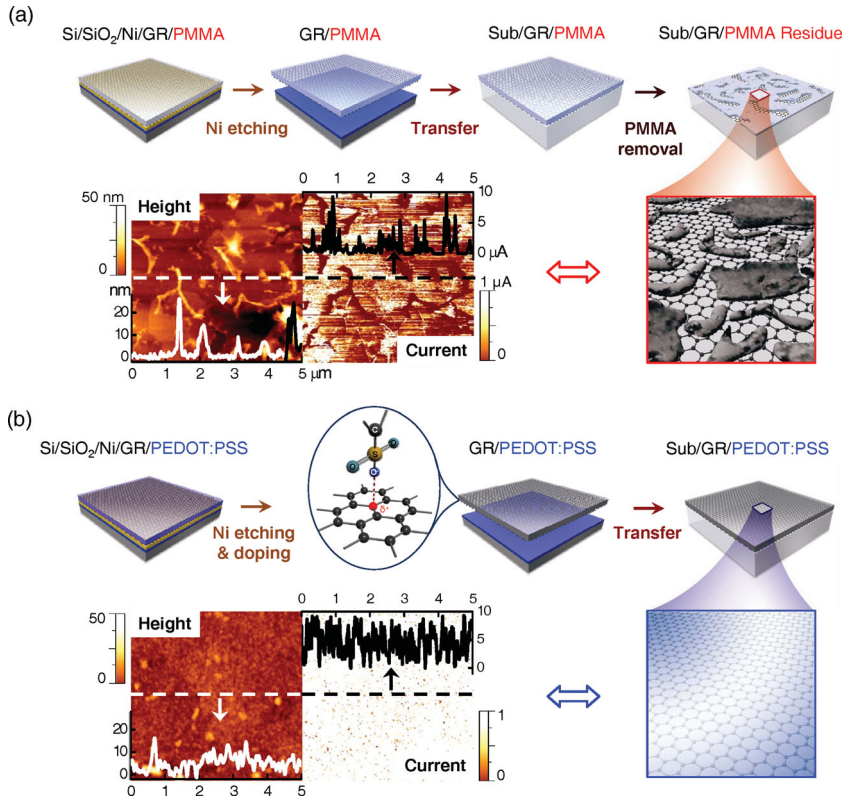

Figure 1. Schematic illustrations and representative c-AFM data for the a) CT and b) DT methods. PMMA (80 nm) and PEDOT:PSS (50 nm) were used as the supporting film in the CT and DT methods, respectively. Representative c-AFM height images (left) and current images (right) for both the CT-GR (a) and DT-GR/P (b) films are shown. The inset graphs show the height and current profiles along the dashed lines. The inserted illustration in (b) shows a doping mechanism of GR by PEDOT:PSS.

in the second category need to be verified for the complete transfer of GR without damage to the film, and require chemical glues for specific target substrates to be specified, which can be cumbersome. The approaches in the third category increase the complexity of the transfer process by adding harsh processes that also prevent the use of delicate substrates, and finally, those in the fourth category retain the complexity of the removal process of the supporting layer. One report in the fourth category showed that the supporting layer can remain on the GR to maintain the GR doping effect.[20] However, the applied supporting layer was also an insulating polymer, which obstructs the charge transfer to GR electrodes. Due to these limitations, none of these reports achieved the implementation of GR's high functionality in polymer solar cells (PSCs) or polymer light-emitting diodes (PLEDs), which are among the most important applications of GR electrodes.[2,3]

Another major issue affecting the preparation of highly functional transparent GR electrodes is stable doping, which has been also a bottleneck for the commercialization of carbon nanotube-based transparent electrodes.[6] Because GR has a very low charge concentration when it is in pristine condition, chemicals must be used to increase the conductivity of GR films.[4,6,22] Unfortunately, commonly used dopants such as HNO_3, or $AuCl_3$ were found to be volatile, resulting in a rapid loss of their doping effect upon exposure to air,[23,24] even though stable doping is required for practical GR electrode applications. Recent two works reported the stable doping effect due to the presence of a supporting polymer[20] or its residues.[21] Another recent work also reported the achievement of stable doping by applying an insulating polymer overcoating.[25] However, the use of insulating polymers in these reports on the surface of GR electrodes deposits obstacles for the charge transfer to the GR electrodes. The recent paper reported the achievement of stable doping using a MoO_x layer on GR,[26] which is used as a hole transport layer (HTL) on GR electrodes of organic solar cells.[11,27] Although this approach results in the practically meaningful stable doping of GR, it requires a separate doping step after the GR transfer. Therefore, it does not decrease the complexity of the GR transfer process or solve the issues, the residues and harsh removal process, of the GR transfer.

Here, we report a new GR transfer process, denoted as 'doping transfer (DT)' method, which solves the issues of GR transfer and doping stability by using poly(3,4-ethylenedioxythiophene):poly(styrenesulfonate) (PEDOT:PSS) as a new supporting layer. Because PEDOT:PSS is a well-known conducting polymer widely used as a HTL or electrode in many organic electronic devices,[9,10,28,29] the GR/PEDOT:PSS bilayer electrodes can be used directly for many applications without removing the supporting layer. Despite these apparent advantages, the well-known water solubility of PEDOT:PSS[30,31] has concealed its potential as a supporting layer in the conventional transfer (CT) processes because these processes involve a water-cleaning step. We found that the interaction with the metal-etching solvent enhanced the water-resistance of the PEDOT:PSS supporting layer during our transfer process,[32,33] and thus the layer remained intact above the GR. Therefore, our new DT method simplifies the GR transfer process significantly while simultaneously eradicating the residue contamination problem observed with CT methods (see Figure 1b). Furthermore, we discovered that the PEDOT:PSS doping of GR is highly stable. Our new GR/PEDOT:PSS electrodes demonstrate better performance compared to the GR electrodes fabricated via the CT method and even comparable to that of the ITO electrodes. Conventional structure PSCs with 5.5% (glass substrate) and 4.8% (flexible substrate) efficiencies and an inverted structure PSC with 6.0% (glass substrate) efficiency were constructed using our new GR/PEDOT:PSS hybrid electrodes. With a simplified transfer process, no residue contamination, and the achievement of stable doping, we expect that our new transfer method will allow GR to become a dominant electrode material in organic electronics.

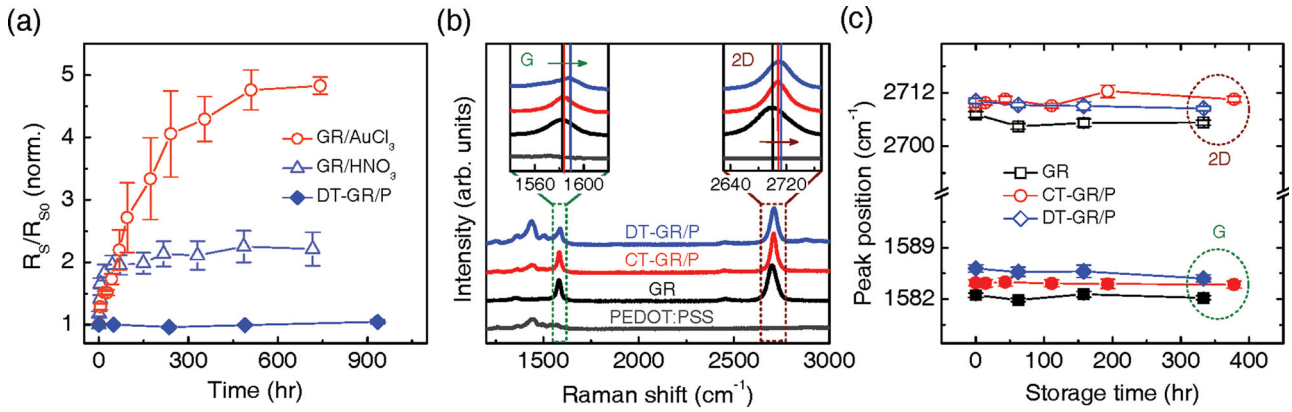

Figure 2. a) The changes in the normalized R_S of GR films ($R_S = 350\ \Omega\ \square^{-1}$) doped with $AuCl_3$ ($R_{S0} = 58\ \Omega\ \square^{-1}$), HNO_3 ($R_{S0} = 224\ \Omega\ \square^{-1}$), and PEDOT:PSS (DT method, $R_{S0} = 145\ \Omega\ \square^{-1}$) as a function of storage time in air. R_{S0} represents the R_S of the GR films immediately after doping. For the $AuCl_3$-doped sample, a 20 mM $AuCl_3$ solution in nitromethane was spin-coated onto the GR films at 2000 rpm for 60 s. For the HNO_3-doped sample, the GR films were immersed in a 5 M aqueous HNO_3 solution for 2 hrs. Note that the doping instability of the dopants is dependent on the doping density and the environmental conditions such as humidity. b) Representative Raman spectra of PEDOT:PSS, GR, CT-GR/P, and DT-GR/P films. The insets show magnified spectra near the G peak and near the 2D peak regions. The blue shifts in the Raman peaks observed here indicate the p-doping of GR by PEDOT:PSS.[52] c) The average Raman peak (G: lower; 2D: upper) positions are plotted as a function of storage time in air. The Raman results confirm that the doping effect was maintained for over 300 h.

2. Results and Discussion

2.1. Simplified Process with the Reduced Contact Resistance

The advantages of GR/PEDOT:PSS electrodes fabricated via the DT method (denoted as DT-GR/P) are illustrated in Figure 1. The DT method simplifies the transfer process due to the absence of the PMMA removal step. The CT method deposited a significant amount of the PMMA residues on the GR (denoted as CT-GR) in the form of either a thin-film coating or randomly shaped lumps that were observed by conductive atomic force microscopy (c-AFM). These nonuniformly distributed PMMA residues significantly hinder the flow of the contact current, resulting in a decrease and wide variation in the average current from 13 nA to 3.5 μA (at a bias of 0.5 V) across six 5 μm × 5 μm measured areas in the CT-GR. In contrast, the DT-GR/P film exhibited high contact current flow with little variation in the average current, which ranged from 4.0 to 5.2 μA. The average contact resistance (R_C) of the measured areas for three types of samples, CT (RA), CT (HA), and DT, were measured for comparison purposes (see Figure S6, Supporting Information). Note that room-temperature acetone (RA) or hot acetone (HA) was used to remove the PMMA from the CT (RA) or CT (HA) samples, respectively. The R_C of the DT sample was almost an order of magnitude lower at 0.11 ± 0.01 MΩ than that of 1.19 ± 0.79 MΩ observed for the CT (RA) sample and 0.66 ± 0.56 MΩ for the CT (HA) sample.

2.2. Stable Doping and the High Transparency

Another important advantage of our approach is that the PEDOT:PSS layer acts as a stable dopant for the GR films. Our as-grown GR films exhibit a sheet resistance (R_S) of 214 ± 22 $\Omega\ \square^{-1}$. Due to the effective doping of the PEDOT:PSS layer, the DT-GR/P film exhibited a 63% decrease in the R_S to 80 ± 4 $\Omega\ \square^{-1}$ (see Figure S8, Supporting Information). The PEDOT:PSS-doped GR exhibited excellent electrical stability in air, as demonstrated in **Figure 2**a. While GR films doped with other popular dopants, such as $AuCl_3$ or HNO_3, rapidly degrade due to the loss of their doping effect as reported,[23,24,34] our DT-GR/P films maintained their low resistance with less than a 5% increase over 934 h. The Raman spectroscopy data shown in Figure 2b,c corroborate these results. The doping effect of PEDOT:PSS on GR has been reported.[35] However, to our knowledge, the actively pursued stable doping of GR[6,20,21,25,26] by PEDOT:PSS has not been reported. The doping of the DT-GR/P film was further increased by applying additional dopants at the bottom surface of the film. By predepositing a PEDOT:PSS layer on the substrate (and briefly immersing the sample in $FeCl_3$ etchant solution and rinsing in DI water to enhance the water resistance) and depositing the DT-GR/P film on top of the PEDOT:PSS layer, the R_S was reduced by an additional 10%, reaching 72 ± 2 $\Omega\ \square^{-1}$. Alternatively, the GR bottom surface could be doped with $HAuCl_4$ by floating the DT-GR/P film on a 2.5 mM aqueous solution for 10 min before transferring to a substrate.[35] In this case, the R_S decreased to 38.6 ± 6.6 $\Omega\ \square^{-1}$. However, the $HAuCl_4$ doping was unstable, similar to the $AuCl_3$ doping, and degraded the morphology of the DT-GR/P films to induce device failure when applied in organic thin film devices.

Another advantage of our DT method arises from the high transparency of PEDOT:PSS.[29] The optical transmittance (T) measurements revealed that the addition of a PEDOT:PSS layer decreased the T value by only 1% (**Figure 3**a). The GR film alone exhibited T values of 85.6% at a wavelength (λ) of 550 nm and maintained the transparency throughout the visible range (400–700 nm). Our Ni-grown GR films displayed lower transparency than the Cu-grown GR films due to the formation of multi-layer domains in the film (see the

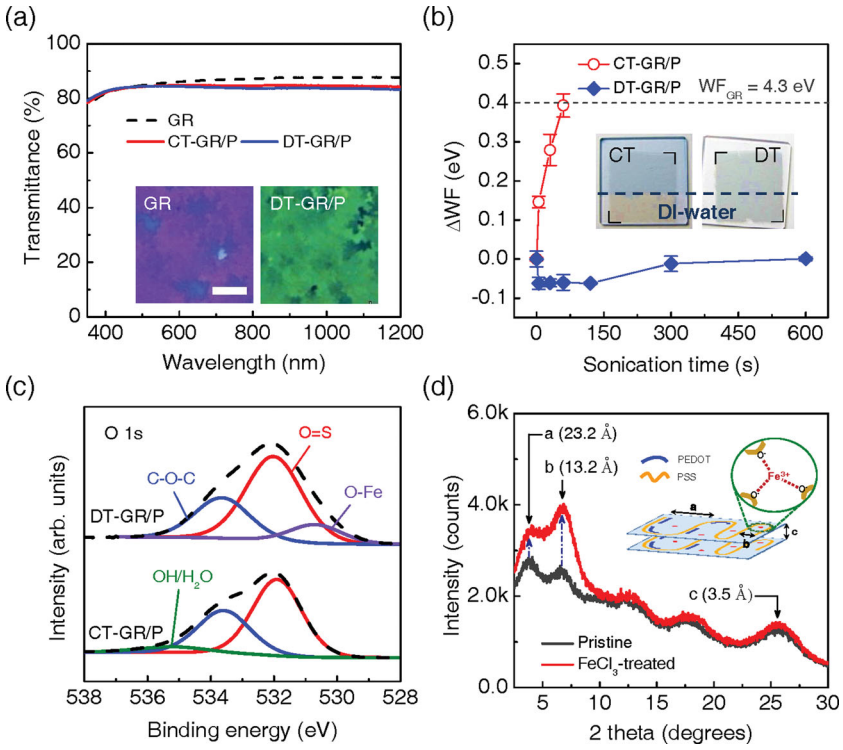

Figure 3. a) Optical transmittance spectra. The insets contain the optical micrographs of the bare (left) and PEDOT:PSS-coated (right) GR films. Scale bar represents 10 µm. b) Changes in the work function (ΔWF) of the CT-GR/P and DT-GR/P films as a function of sonication time in DI water. The insets show photographs of the CT-GR/P (left) and DT-GR/P (right) films on fused silica substrates (area = 2 cm × 2 cm) after partial immersion and sonication in DI water for 30 s. The dashed line indicates the immersion boundary. c) XPS spectra from the CT-GR/P (lower lines) and DT-GR/P (upper lines) films near the O 1s core levels. The spectra of the two samples were markedly different. The sub-peak for the OH/H_2O bond (535 eV) could be differentiated in the spectra of the CT sample, but not in the spectra of the DT sample. Furthermore, the sub-peak representing the O-Fe bond (530.6 eV) was only observed in the DT sample.[53] d) XRD spectra of the PEDOT:PSS films in the presence (red line) and absence (gray line) of the $FeCl_3$ vapor treatment. The inset illustrates our hypothesis regarding the interaction between the Fe ions and the PSS chains.

inset of Figure 3a).[4,7] The multilayered structure makes our Ni-GR films easier to handle because of their higher mechanical strength in comparison to the Cu-GR films. Due to the high transparency of PEDOT:PSS, our DT-GR/P film is a good candidate for transparent electrodes in optoelectronic devices.[2,3,6]

2.3. Increased Mechanical Robustness and Work Function

Additional advantages were achieved with our DT method. The mechanical robustness of the PEDOT:PSS layer in the DT-GR/P films in the presence of water was increased after the DT process to the extent that it was able to withstand the ultrasonication treatment, as shown in the inset of Figure 3b. A similar change in the water solubility of PEDOT:PSS using a solvent-bath treatment has been reported before.[36] Such an increase is beneficial in terms of the mass production processes of organic devices,[37,38] because it allows for the use of environmentally benign water-based functional materials[39] on top of the PEDOT:PSS layer overcoming the issue of solvent orthogonality.[37,40] We utilized this advantage when fabricating the inverted structure PSCs as discussed below. The work function of the DT-GR/P and CT-GR/P samples were measured by Kelvin probe measurements as a function of ultrasonication time; the results are shown in Figure 3b (see also Figure S9, Supporting Information). This increase in the robustness is due to two effects: the strong cohesion between PEDOT:PSS and GR and the increased cohesion within the PEDOT:PSS layer. The first effect is likely due to the strong attraction between the sulfonic acid group of PSS and GR as discussed in more detail below. In contrast, the $FeCl_3$-treated PEDOT:PSS layer on ITO could be easily detached from ITO by sonication in water. Such strong cohesion may also foster charge transfer between PEDOT:PSS and GR in the DT-GR/P film, thereby increasing its functionality as an electrode. The second effect is likely associated with the crosslinking effect of the PSS chains induced by the Fe^{3+} ions adsorbed from $FeCl_3$ vapor during the DT process (see the illustration in Figure 3d).[32,33] The Fe^{3+} ion can induce the ordering of the PSS excess chains, which are responsible for the water solubility, by forming a $3(S(=O)_2\text{-}O^-)$–Fe^{3+} structure. In this manner, the water miscibility is reduced.[32,33]

Our hypothesis is supported by the X-ray photoelectron spectroscopy (XPS) data which detected the Fe element (see Figure S10, Supporting Information) and showed a decrease in the signal from the OH group and the presence of a signal from the O-Fe group in the DT-GR/P film (see Figure 3c and Figure S11, Supporting Information). Another source of evidence was obtained from the X-ray diffraction (XRD) patterns of 25-µm-thick PEDOT:PSS films in the absence and presence of a $FeCl_3$ vapor (five-day exposure) treatment (see Figure 3d). Exposure to $FeCl_3$ vapor resulted in an enhanced peak intensity at $2\theta = 3.8$ and 6.7°, which correspond to PEDOT:PSS lamella stacking distances of 23.2 and 13.2 Å, respectively (see the inset of Figure 3d).[41,42] Note that only few reports recently identified structural changes in the PEDOT:PSS solid films by XRD spectroscopy[41,42] including one from our group.[41]

The absorption of Fe in the PEDOT:PSS also resulted in another advantage of our DT method, which involves an increase in the work function of the DT-GR/P film (5.4 eV) compared to that (5.2 eV) of the CT-GR/P film (see Figure S12, Supporting Information). The higher work function of our DT-GR/P films is advantageous for anodes in organic devices that use p-type materials with high ionization energy.[24,43] This increase in the work function can be induced by a change in the Madelung potential of the ion structure in the PEDOT:PSS by the Fe^{3+} ion.[33]

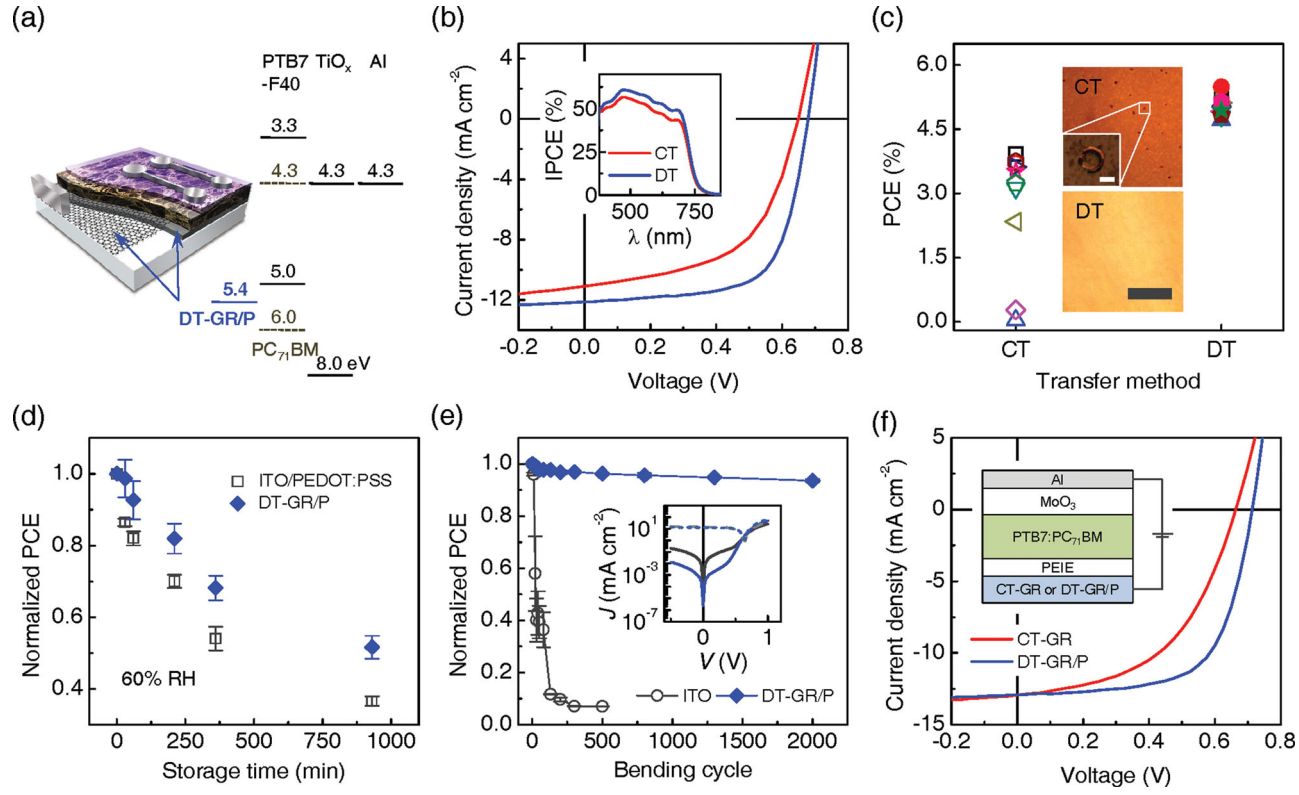

Figure 4. a) Schematic illustrating the structure and corresponding energy-level diagram of the fabricated conventional structure PSC. For some of the devices, an additional PEDOT:PSS layer (Al 4083, 30 nm) was used with the DT-GR/P electrode. b) The current density-voltage (*J–V*) characteristics of the best solar cells with the CT-GR (red line) and the DT-GR/P (blue line) electrodes under simulated AM 1.5 G radiation at 100 mW cm^{-2}. The inset shows the incident photon-to-current efficiency (IPCE) spectra of the devices. c) PCEs of the PSCs fabricated with the CT-GR (open symbols) and the DT-GR/P (closed symbols) electrodes. The insets reveal the optical micrographs of the PEDOT:PSS surfaces of the CT-GR/P (top) and the DT-GR/P (bottom) films after depositing pure chlorobenzene. Scale bars represent 10 µm (white) and 300 µm (grey) respectively. d) Normalized variations in the PCEs of the conventional structure PSCs (with a PTB7:$PC_{71}BM$ active layer) with the DT-GR/P (closed diamonds, without an additional PEDOT:PSS layer) and the ITO (open squares) electrodes as a function of storage time in air (RH 60%). e) Normalized PCE of flexible PSCs with the DT-GR/P (closed symbols) and the ITO (open symbols) anodes. The inset is a semi-log *J–V* plot of flexible devices containing the ITO (gray lines) and the DT-GR/P (blue lines) electrodes both in the presence (dashed lines) and absence (solid lines) of irradiation. f) The *J–V* characteristics of the best inverted structure PSCs with the CT-GR (red line) and the DT-GR/P (blue line) electrodes. The inset represents the device structure of the inverted PSCs. The R_S values of the used electrodes were: CT-GR (≈ 350 Ω □$^{-1}$ for a-e devices and ≈ 214 Ω □$^{-1}$ for f devices); DT-GR/P (≈145 Ω □$^{-1}$ for a–e devices and ≈80 Ω □$^{-1}$ for f devices); ITO (≈ 15 Ω □$^{-1}$ on glass and ≈ 60 Ω □$^{-1}$ on PET).

2.4. High Performance as Electrodes in Polymer Solar Cells

To investigate the application of the DT-GR/P films as electrodes in organic devices, we fabricated bulk heterojunction (BHJ) PSCs in conventional structure, as shown in **Figure 4**a (see Figure S13, Supporting Information) using the DT-GR/P electrodes, as well as the CT-GR and ITO electrodes for comparison. The current density-voltage (*J–V*) measurements demonstrated excellent device performance for the DT-GR/P devices, which exhibited the highest PCE of 5.5% and fill factor (FF) of 0.67. This PCE value is, to our knowledge, the highest value reported for conventional structure PSCs using GR electrodes to date (see Table S3, Supporting Information).[9–12] The average PCE value was 1.8 times higher than that of the reference CT-GR devices (the highest PCE = 3.9% and FF = 0.55) as shown in **Table 1** and Figure 4b. The improved PCE is mostly due to the elimination of PMMA residues, which increase the R_C and worsen the surface morphology, as discussed above. Remarkably, the best DT-GR/P device yielded a FF of 0.67, which was even higher than that (FF = 0.61) of the best ITO device (PCE = 5.9%), despite the higher R_S of the DT-GR/P film relative to ITO. Benefitting from the improved FF, the best DT-GR/P device showed a comparable PCE value (93%, also one of the highest ratios among recent reports, see Table S3, Supporting Information) to the best ITO device. This ratio was 84% when compared by the average PCEs. Note that the higher absolute PCE for our DT-GR/P device compared to those reported for conventional structure PSCs with GR electrodes[9–12] is dependent on the use of an efficient active material, PTB7-F40:$PC_{71}BM$. The observed superb compatibility of the DT-GR/P hybrid electrodes with such highly efficient active material increases the potential of our electrodes for applications in highly efficient and commercially viable PSCs. Furthermore, we examined the advantages of our method through comparisons with reference ITO devices, as reported in previous studies.[9,11,12] The improvement in the FF is mainly due

Table 1. Performance parameters of the devices fabricated in this study. All parameters are from the best devices except the average PCE values. Note that two different GRs (denoted as GR1 and GR2) were used in the device fabrications as indicated in the table. Their synthesis conditions were slightly different and their R_S values were also different: GR1 ≈ 350 Ω □$^{-1}$ and GR2 ≈ 214 Ω □$^{-1}$ (see the Supporting Information for more details).

							PCE [%]	
Device structure	Active material	Substrate	Electrode	V_{oc} (V)	J_{sc} [mA cm^{-2}]	FF	Average	Best
Conventional cell	PTB7-F40:$PC_{71}BM$	Glass	ITO	0.68	14.1	0.61	5.8 ± 0.1	5.9
			CT-GR1/P	0.65	11.1	0.55	2.7 ± 1.8	3.9
			DT-GR1/P	0.68	12.1	0.67	4.9 ± 0.2	5.5
		PET	ITO	0.64	14.3	0.52	4.5 ± 0.2	4.7
			DT-GR1/P	0.64	12.5	0.60	4.6 ± 0.2	4.8
Inverted cell	PTB7:$PC_{71}BM$	Glass	ITO	0.72	14.0	0.67	6.8 ± 0.1	6.8
			CT-GR2	0.66	12.9	0.50	3.9 ± 0.5	4.3
			DT-GR2/P	0.71	12.9	0.65	5.7 ± 0.3	6.0

to the enhanced shunt resistance of the DT-GR/P device (R_{sh} ≈ 846 Ω cm^2) relative to the ITO device (R_{sh} ≈ 290 Ω cm^2; see Figure S14, Supporting Information). The series resistances were 6.7 Ω cm^2 for the DT-GR/P electrode and 4.4 Ω cm^2 for the ITO electrode. The higher series resistance of the DT-GR/P device was due to the higher R_S value of the DT-GR electrode compared to the ITO electrode. However, the 3-times improvement of the shunt resistance affected the FF dominantly compared to the 1.5-times decline of the series resistance in these two devices. The generality of the advantage in using our DT-GR/P electrode in conventional structure PSCs was examined by fabricating PSCs using a different high-efficiency active material, PCDTBT:$PC_{71}BM$, with similar results. The average PCE of the DT-GR/P devices was 1.6 times higher than that of the CT-GR devices and 20% lower than that of the ITO devices (Figure S15 and Table S4, Supporting Information).

2.5. Reproducible Device Fabrication and Enhanced Device Lifetime

Importantly, we observed that device fabrication using DT-GR/P exhibited excellent reproducibility. We fabricated 10 devices using DT-GR/P and 10 using CT-GR/P and compared their PCE distribution, as shown in Figure 4c. Although we tried to fabricate these devices under identical conditions, the CT-GR/P devices exhibited low reproducibility, with widely varying PCE values (PCE ≈ 0–4%). However, the DT-GR/P devices exhibited excellent reproducibility with only small variations in their PCE values (4.9 ± 0.2%). The large PCE variation in the CT-GR/P devices was induced by the randomly distributed PMMA residues. Furthermore, we observed an additional harmful effect of the PMMA residue. While spin-coating the active layer, the solvent (chlorobenzene) penetrated the PEDOT:PSS layer and dissolved the PMMA residues, which created swelled deformations of up to a few micrometers in height that were sporadically scattered throughout the functional region of the CT-GR/P devices, as shown in the insets of Figure 4c. Such deformations can reduce the device performance or even cause device failure by creating an electrical short on that location.

We also found that the use of our DT-GR/P electrodes improved the device lifetime. The PEDOT:PSS layer in PSCs is known to induce a device stability problem because the acidic excess PSS can diffuse to other layers and induce interface instability.[27] Because the excess PSS in the PEDOT:PSS layer is fixated by the Fe^{3+} ions during the DT process, as discussed above, an enhancement in the lifetime is expected for PSCs using the DT-GR/P electrodes. To verify this expectation, the lifetime of conventional structure PSCs using DT-GR/P electrodes was monitored and compared against that of the reference ITO devices with a pristine PEDOT:PSS layer (Figure 4d). The results demonstrated that the DT-GR/P devices had an enhanced device lifetime and retained 52% of the initial PCE after storage in room air of 60% relative humidity (RH) for 930 min, a 1.4-fold increase over the 37% retention ratio of the reference ITO devices.

2.6. High Performance as Electrodes onto Flexible Substrates

One of the main advantages of GR electrodes is their mechanical flexibility.[1–3] To assess the performance of the DT-GR/P films as a flexible electrode, we fabricated flexible PSCs of a conventional structure on poly(ethylene terephthalate) (PET) substrates. We also fabricated reference solar cells using ITO-coated PETs. The flexible DT-GR/P devices exhibited the highest PCE (4.8%), as shown in Table 1 and the inset of Figure 4e, which again is the highest reported value for flexible PSCs prepared using GR electrodes[10] and is even better than the PCE of the best reference ITO device (4.7%; 102% ratio by either the best PCEs or the average PCEs, see Table 1 and Table S3 in the Supporting Information). The FF value for the flexible DT-GR/P device (0.60) was also much higher than that of the flexible ITO device (0.52). Such an increase in the FF and consequent improvement in the PCE value of the flexible DT-GR/P device in comparison to the ITO device can be attributed to the smaller R_S difference between the DT-GR/P film and ITO film on PET, in addition to the above-mentioned factors. Furthermore, the flexible DT-GR/P PSCs performed much better than the flexible ITO devices under a bending

stress, confirming the previously reported results.[10] Figure 4e compares the normalized PCEs of both devices as a function of bending cycles. Due to the brittle nature of ITO electrodes, the PCE of the flexible ITO device decreased by 60% after only 30 bending cycles (bending radius ≤ 5 mm), and the device nearly ceased functioning after 500 bending cycles. In contrast, the PCE of the flexible DT-GR/P device was reduced by only 6% even after 2000 bending cycles. These results demonstrate the superior performance of the DT-GR/P electrodes fabricated via our DT method in flexible PSCs.

2.7. Inverted Polymer Solar Cells and Polymer Light-Emitting Diodes

The high work function of the GR electrode makes it suitable for use as an anode, which inject or extract hole charge carriers, in organic devices.[24,43] The addition of a PEDOT:PSS layer further increases the work function to increase its effectiveness as an anode, as discussed above. Therefore, our DT-GR/P hybrid electrode performs well as an anode without the addition of a HTL in PSCs, as described above. However, the cathode application of the GR electrodes is a particularly important aspect for inverted structure PSCs.[13] The inverted structure increases the device lifetime and flexibility in device design such as tandem structure devices.[13] To use GR as cathodes, researchers have utilized work-function-lowering interfacial layers or electron transport layers (ETLs).[13] Recently, simple and highly efficient work-function-lowering polymers were reported, including by our group.[44]

To investigate the performance of our DT-GR/P film as a cathode in inverted structure PSCs, we utilized the recently developed polyethylenimine ethoxylated (PEIE)[44] as a cathode interfacial layer in the device structure, as shown in the inset of Figure 4f. In depositing the PEIE layer from an aqueous solution on the DT-GR/P electrodes, the increased mechanical strength of the PEDOT:PSS layer against water during the DT process, as mentioned above, was a critical factor. Representative *J*–*V* curves from devices using the CT-GR and DT-GR/P electrodes are shown in Figure 4f. As with the conventional structure devices discussed above, we also observed the 1.5-fold higher average PCE values for the DT-GR/P devices in comparison to the CT-GR devices, which correspond to 84% of the average PCE of the ITO devices (Table 1). Interestingly, the best PCE of the DT-GR/P devices was 6.0%, which is higher than that of the best conventional structure device reported above and is the highest value reported thus far for inverted structure PSCs using GR electrodes (Table S3, Supporting Information).[13] We attribute the high performance of the DT-GR/P electrodes in inverted structure PSCs to the beneficial effects of our DT process, as discussed above, the effectiveness of the PEIE in lowering the work function, and the usage of a highly efficient active material, PTB7:$PC_{71}BM$. The high performance of our DT-GR/P electrodes, even as cathodes in inverted structure PSCs, vastly expands the range of applications for our developed DT technique.

To further investigate the application range of our DT-GR/P electrodes, we also fabricated PLEDs using the DT-GR/P electrodes and a poly(*p*-phenylene vinylene) derivative (Super Yellow, SY; see Figure S13, Supporting Information) for the light-emitting layer and compared them against the ITO electrode devices (Table S5, Figures S16,S17, Supporting Information). The maximum luminous efficiencies (LEs) were similar for both devices (1.9 lm W^{-1}). However a lower turn-on voltage (V_T = 4.0 V) and higher LE in the lower operating voltage range (4–7 V) were observed for the DT-GR/P devices than for the ITO devices (V_T = 4.5 V) (see Figure S16, Supporting Information). A low V_T and high LE at low voltages reduce the Joule heating and enhance the operational lifetime of the PLEDs.[45] The improved PLED performance for the DT-GR/P devices was attributed to the deeper work function of DT-GR/P (5.4 eV) compared to that of ITO (4.4 eV) which foster the charge injection as explained above. These results also indicate that our DT method can be used to fabricate high-performance PLEDs with GR electrodes.

2.8. Single-Layer Graphene Transfer

The performance of the PEDOT:PSS supporting and doping layer with GR was investigated with single-layer GRs (denoted as SLGRs) grown on Cu foils.[4,8] The high transparency of a SLGR is beneficial for applications as transparent electrodes. As observed for the multilayer GRs, we observed that the PEDOT:PSS layer can also be used as a supporting layer during the transfer (due to the effect of the Fe^{3+} ions) and as a combined doping layer after the transfer to reduce the R_S. Furthermore, stacking of multiple DT-SLGR/P layers was achieved, as shown by the representative image in the inset of **Figure 5**a. This stacking was also enabled by the increased water resistance of the PEDOT:PSS layer during the DT process. The transparency values were 95.9, 90.6, 85.3, and 79.9% for 1, 2, 3, and 4 layers of DT-SLGR/P, respectively. The respective R_S values were 650 ± 160, 280 ± 20, 158 ± 3, and 127 ± 1 Ω □$^{-1}$ (Figure 5b). The R_S value was reduced by an additional $HAuCl_4$ doping step, as discussed above, reaching 440 ± 40, 155 ± 7, 111 ± 2, and 76 ± 1 Ω □$^{-1}$, respectively. The R_S of the one-layer CT-SLGR film was 1080 ± 190 Ω □$^{-1}$. We note that the use of the PEDOT:PSS as a supporting layer for the transfer of the SLGRs requires delicate

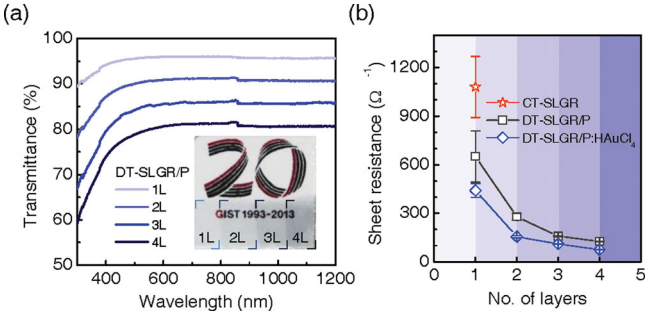

Figure 5. a) Optical transmittance spectra of one- to four-layer DT-SLGR/P films. The inset shows a photograph of an offset-stack of four DT-SLGR/P layers on a fused silica substrate. In the inset, the number of layers in each area is marked. b) Variations in the R_S of the CT-SLGR (star), DT-SLGR/P (squares), and $HAuCl_4$-doped DT-SLGR/P (diamonds) films as a function of the number of layers.

processing control during the transfer, as discussed further in the Supporting Information (see Figures S4,S5). The successful demonstration of our DT method with the SLGRs further highlights the potential of our developed technique for GR applications in optoelectronic devices.

2.9. Doping Mechanisms of GR by PEDOT:PSS

The doping effect of PEDOT:PSS on GR can be induced via three mechanisms: a) electron attraction to the sulfonic acid ($S(=O)_2$–OH) group of PSS chains from GR (acidic doping, as illustrated in Figure 1b).[31] Note that doping with PSS alone decreased the R_S by 22% (see Figure S7, Supporting Information). b) Electron transfer from GR to PEDOT:PSS due to a difference in the work function (charge-transfer doping).[35] Finally, c) bypasses for the charge created via percolation doping through a conductive PEDOT:PSS film across resistive grain boundaries in the GR.[46] We also note that the inclusion of an $FeCl_3$-treated PEDOT:PSS layer below the CT-GR films reduced the R_S by 28% (see Figure S8, Supporting Information). Because the excess PSS was fixated by the Fe^{3+} ions, the main doping effect in this case should be the charge-transfer doping and the percolation doping. We expect that the percolation doping effect to be minimal because the conductivity of the PEDOT:PSS layer used is very low, 0.5 S cm^{-1} (Figure S7, Supporting Information). Therefore, we conclude that both the acidic doping and the charge-transfer doping are similarly effective for GR doping by the PEDOT:PSS layer. The doping stability can be attributed to the environmental stability of PEDOT:PSS[30,47] and the chemical robustness of GR.[3]

2.10. Mechanism for Fill Factor Enhancement

The enhancement of the FFs by using the DT-GR/P electrodes in PSCs can be induced by two factors: 1) the absence of the In diffusion from ITO into the active layer, which creates the exciton quenching sites,[24,48] or 2) the reduction in the proton diffusion from PEDOT:PSS into the active layer, which also creates the exciton quenching sites.[49] The second factor can be induced by a decrease in the proton density in the entire PEDOT:PSS layer (50-nm DT layer + 30-nm added layer) of the DT-GR/P device due to the interaction between the Fe^{3+} ions and the hygroscopic and acidic functionality (–OH) of the PSS, as discussed above (see the inset of Figure 3d and Figure S15 in the Supporting Information). Notably, a performance improvement by the $FeCl_3$ vapor-treatment on the PEDOT:PSS layer was observed with the CT-GR devices (Figure S15 and Table S4, Supporting Information), supporting our assumptions regarding the effect of the $FeCl_3$ vapor exposure on the PEDOT:PSS layer during the DT process on the final device performance. Also, these factors contributed for the observed device lifetime enhancement in Figure 4d.

3. Conclusions

We have developed a new transfer method for CVD-synthesized graphene films by using a commonly-used functional conducting polymer as a supporting layer for the transfer and also as a stable doping layer for graphene. Our method presents a genuine solution to the residue problem of the transfer while providing a stable doping environment for graphene films. The benefits of the simplified process, the removal of insulating residues, the stable doping effect, and other advantages from the synergetic interaction between the conducting polymer and the etchant vapor during the transfer such as increased mechanical strength and deepened work function made it possible for us to fabricate high-performance polymer solar cells and light-emitting diodes with graphene-polymer hybrid electrodes. Our results may contribute to the broad application of fully functional graphene electrodes in organic optoelectronics.

4. Experimental Section

Graphene Growth and Transfer: Multilayer graphene was grown by CVD using a method similar to that reported previously.[50] PMMA was spin-coated (4000 rpm, 35 s) onto the synthesized graphene for transfer via the CT method. The Ni layer was then etched in an aqueous $FeCl_3$ (0.2 M)/HCl (1.1 M) solution for approximately 2 h, and the graphene/PMMA was washed with distilled (DI) water, transferred to the target surface, and dried. The PMMA was then removed by immersing the sample in either room-temperature or hot (80 °C) acetone and subsequently rinsing with IPA and DI water. For the DT method, PEDOT:PSS (PH1000) was spin-coated (7000 rpm, 40 s, for 25 nm thickness) onto UV-O_3–treated (3 mW, 10 min) graphene and then baked on a hot plate at 150 °C for 10 min. The rest of the process was identical to the CT method, except that the PMMA removal process was excluded. Single layer graphene on Cu was purchased from Graphenesquare, Inc. and was transferred by using the CT and the DT method (see the Supporting Information for more details).

Graphene/PEDOT:PSS Characterization: The transmittances was measured using a UV/Visible/NIR spectrophotometer (Lambda 750, PerkinElmer, Inc.). Hall measurements were performed using a system from Bio-Rad, Inc. Raman spectroscopy was performed using an inVia Raman Microscope system from Renishaw, Inc., with an Ar^+ ion laser operating at 514 nm and 1.2 mW. The c-AFM measurements were made using a XE-100 from Park Systems, Inc. Before the measurements, the DT-GR/P samples were heated on a hot plate at 80 °C for 10 min. The work functions were measured using a KP 6500 Digital Kelvin probe, McAllister Technical Services. Co. The UPS measurements were performed using a UPS analysis chamber (1×10^{-9} Torr) equipped with an AXIS-NOVA hemispherical electron energy analyzer with a He I ($h\nu$ = 21.2 eV) source. The samples were kept under high vacuum overnight before the UPS measurements, and a sample bias of –15 V was used. The XRD patterns were obtained from a Rigaku D/max-2500 diffractometer with a conventional θ–2θ geometry using Cu-Kα radiation (λ = 1.540593 Å) at 40 kV and 100 mA.

Polymer Device Fabrication and Characterization: The PSCs and PLEDs were fabricated using previously reported procedures.[51] The device performances were measured using a Keithley 238 Source Measure Unit (see the Supporting Information for more details).

Supporting Information

Supporting Information is available from the Wiley Online Library or from the author.

Acknowledgements

B.H.L. and J.-H.L. contributed equally to this work. The authors thank the Heeger Center for Advanced Materials (HCAM) at GIST for their

assistance with the measurements. This work was supported by the Core Technology Development Program for Next-Generation Solar Cells of the Research Institute for Solar and Sustainable Energies (RISE) at GIST and the National Research Foundation (NRF) of Korea (2008–0093869 and 2008–0062606 (CELA-NCRC)). The authors are grateful to A. J. Heeger at the UCSB for his valuable advice and discussion.

Received: August 21, 2013
Revised: October 3, 2013
Published online: November 27, 2013

[1] a) K. S. Novoselov, A. K. Geim, S. V. Morozov, D. Jiang, Y. Zhang, S. V. Dubonos, I. V. Grigorieva, A. A. Firsov, *Science* **2004**, *306*, 666; b) A. K. Geim, *Science* **2009**, *324*, 1530.

[2] F. Bonaccorso, Z. Sun, T. Hasan, A. C. Ferrari, *Nat. Photonics* **2010**, *4*, 611.

[3] S. Pang, Y. Hernandez, X. Feng, K. Müllen, *Adv. Mater.* **2011**, *23*, 2779.

[4] S. Bae, H. Kim, Y. Lee, X. Xu, J.-S. Park, Y. Zheng, J. Balakrishnan, T. Lei, H. R. Kim, Y. I. Song, Y.-J. Kim, K. S. Kim, B. Özyilmaz, J.-H. Ahn, B. H. Hong, S. Iijima, *Nat. Nanotechnol.* **2010**, *5*, 574.

[5] J. Kang, D. Shin, S. Bae, B. H. Hong, *Nanoscale* **2012**, *4*, 5527.

[6] D. S. Hecht, L. Hu, G. Irvin, *Adv. Mater.* **2011**, *23*, 1482.

[7] a) X. Li, W. Cai, J. An, S. Kim, J. Nah, D. Yang, R. Piner, A. Velamakanni, I. Jung, E. Tutuc, S. K. Banerjee, L. Colombo, R. S. Ruoff, *Science* **2009**, *324*, 1312; b) A. Reina, X. Jia, J. Ho, D. Nezich, H. Son, V. Bulovic, M. S. Dresselhaus, J. Kong, *Nano Lett.* **2009**, *9*, 30; c) K. S. Kim, Y. Zhao, H. Jang, S. Y. Lee, J. M. Kim, K. S. Kim, J.-H. Ahn, P. Kim, J.-Y. Choi, B. H. Hong, *Nature* **2009**, *457*, 706.

[8] a) Z. Yan, J. Lin, Z. Peng, Z. Sun, Y. Zhu, L. Li, C. Xiang, E. L. Samuel, C. Kittrell, J. M. Tour, *ACS Nano* **2012**, *6*, 9110; b) R. S. Weatherup, B. Dlubak, S. Hofmann, *ACS Nano* **2012**, *6*, 9996.

[9] a) M. Choe, B. H. Lee, G. Jo, J. Park, W. Park, S. Lee, W.-K. Hong, M.-J. Seong, Y. H. Kahng, K. Lee, T. Lee, *Org. Electron.* **2010**, *11*, 1864; b) b) H. Park, P. R. Brown, V. Bulović, J. Kong, *Nano Lett.* **2012**, *12*, 133.

[10] a) L. Gomez De Arco, Y. Zhang, C. W. Schlenker, K. Ryu, M. E. Thompson, C. Zhou, *ACS Nano* **2010**, *4*, 2865; b) S. Lee, J.-S. Yeo, Y. Ji, C. Cho, D.-Y. Kim, S.-I. Na, B. H. Lee, T. Lee, *Nanotechnology* **2012**, *23*, 344013.

[11] Y. Wang, S. W. Tong, X. F. Xu, B. Özyilmaz, K. P. Loh, *Adv. Mater.* **2011**, *23*, 1514.

[12] H. Park, R. M. Howden, M. C. Barr, V. Bulović, K. Gleason, J. Kong, *ACS Nano* **2012**, *6*, 6370.

[13] a) G. Jo, S.-I. Na, S.-H. Oh, S. Lee, T.-S. Kim, G. Wang, M. Choe, W. Park, J. Yoon, D.-Y. Kim, Y. H. Kahng, T. Lee, *Appl. Phys. Lett.* **2010**, *97*, 213301; b) D. Zhang, F. Xie, P. Lin, W. C. H. Choy, *ACS Nano* **2013**, *7*, 1740; c) H. Park, S. Chang, M. Smith, S. Gradecak, J. Kong, *Sci. Rep.* **2013**, *3*, 1581.

[14] a) Z. Cheng, Q. Zhou, C. Wang, Q. Li, C. Wang, Y. Fang, *Nano Lett.* **2011**, *11*, 767; b) Y.-C. Lin, C.-C. Lu, C.-H. Yeh, C. Jin, K. Suenaga, P.-W. Chiu, *Nano Lett.* **2012**, *12*, 414.

[15] a) J. Hofrichter, B. u. N. Szafranek, M. Otto, T. J. Echtermeyer, M. Baus, A. Majerus, V. Geringer, M. Ramsteiner, H. Kurz, *Nano Lett.* **2010**, *10*, 36; b) H.-J. Shin, W. M. Choi, S.-M. Yoon, G. H. Han, Y. S. Woo, E. S. Kim, S. J. Chae, X.-S. Li, A. Benayad, D. D. Loc, F. Gunes, Y. H. Lee, J.-Y. Choi, *Adv. Mater.* **2011**, *23*, 4392; c) Z. Yan, Z. Peng, Z. Sun, J. Yao, Y. Zhu, Z. Liu, P. M. Ajayan, J. M. Tour, *ACS Nano* **2011**, *5*, 8187; d) Z. Peng, Z. Yan, Z. Sun, J. M. Tour, *ACS Nano* **2011**, *5*, 8241; e) T. Kato, R. Hatakeyama, *ACS Nano* **2012**, *6*, 8508; f) W. Xiong, Y. S. Zhou, L. J. Jiang, A. Sarkar, M. Mahjouri-Samani, Z. Q. Xie, Y. Gao, N. J. Ianno, L. Jiang, Y. F. Lu, *Adv. Mater.* **2013**, *25*, 630; g) J. Chen, Y. Guo, Y. Wen, L. Huang, Y. Xue, D. Geng, B. Wu, B. Luo, G. Yu, Y. Liu, *Adv. Mater.* **2013**, *25*, 992.

[16] a) R. Bajpai, S. Roy, L. Jain, N. Kulshrestha, K. S. Hazra, D. S. Misra, *Nanotechnology* **2011**, *22*, 225606; b) E. H. Lock, M. Baraket, M. Laskoski, S. P. Mulvaney, W. K. Lee, P. E. Sheehan, D. R. Hines, J. T. Robinson, J. Tosado, M. S. Fuhrer, S. C. Hernández, S. G. Walton, *Nano Lett.* **2012**, *12*, 102.

[17] Y.-D. Lim, D.-Y. Lee, T.-Z. Shen, C.-H. Ra, J.-Y. Choi, W. J. Yoo, *ACS Nano* **2012**, *6*, 4410.

[18] X. Liang, B. A. Sperling, I. Calizo, G. Cheng, C. A. Hacker, Q. Zhang, Y. Obeng, K. Yan, H. Peng, Q. Li, X. Zhu, H. Yuan, A. R. Hight Walker, Z. Liu, L.-m. Peng, C. A. Richter, *ACS Nano* **2011**, *5*, 9144.

[19] a) Y.-C. Lin, C. Jin, J.-C. Lee, S.-F. Jen, K. Suenaga, P.-W. Chiu, *ACS Nano* **2011**, *5*, 2362; b) M. G. Lemaitre, E. P. Donoghue, M. A. McCarthy, B. Liu, S. Tongay, B. Gila, P. Kumar, R. K. Singh, B. R. Appleton, A. G. Rinzler, *ACS Nano* **2012**, *6*, 9095.

[20] G.-X. Ni, Y. Zheng, S. Bae, C. Y. Tan, O. Kahya, J. Wu, B. H. Hong, K. Yao, B. Özyilmaz, *ACS Nano* **2012**, *6*, 3935.

[21] W. H. Lee, J. W. Suk, J. Lee, Y. Hao, J. Park, J. W. Yang, H.-W. Ha, S. Murali, H. Chou, D. Akinwande, K. S. Kim, R. S. Ruoff, *ACS Nano* **2012**, *6*, 1284.

[22] J. O. Hwang, J. S. Park, D. S. Choi, J. Y. Kim, S. H. Lee, K. E. Lee, Y.-H. Kim, M. H. Song, S. Yoo, S. O. Kim, *ACS Nano* **2012**, *6*, 159.

[23] K. K. Kim, A. Reina, Y. Shi, H. Park, L.-J. Li, Y. H. Lee, J. Kong, *Nanotechnology* **2010**, *21*, 285205.

[24] T.-H. Han, Y. Lee, M.-R. Choi, S.-H. Woo, S.-H. Bae, B. H. Hong, J.-H. Ahn, T.-W. Lee, *Nat. Photonics* **2012**, *6*, 105.

[25] C. Yan, K.-S. Kim, S.-K. Lee, S.-H. Bae, B. H. Hong, J.-H. Kim, H.-J. Lee, J.-H. Ahn, *ACS Nano* **2012**, *6*, 2096.

[26] S. L. Hellstrom, M. Vosgueritchian, R. M. Stoltenberg, I. Irfan, M. Hammock, Y. B. Wang, C. Jia, X. Guo, Y. Gao, Z. Bao, *Nano Lett.* **2012**, *12*, 3574.

[27] Y. Sun, C. J. Takacs, S. R. Cowan, J. H. Seo, X. Gong, A. Roy, A. J. Heeger, *Adv. Mater.* **2011**, *23*, 2226.

[28] a) J. Ouyang, C. W. Chu, F. C. Chen, Q. Xu, Y. Yang, *Adv. Funct. Mater.* **2005**, *15*, 203; b) W. Gaynor, G. F. Burkhard, M. D. McGehee, P. Peumans, *Adv. Mater.* **2011**, *23*, 2905.

[29] Y. Xia, K. Sun, J. Ouyang, *Adv. Mater.* **2012**, *24*, 2436.

[30] L. Groenendaal, F. Jonas, D. Freitag, H. Pielartzik, J. R. Reynolds, *Adv. Mater.* **2000**, *12*, 481.

[31] X. Crispin, S. Marciniak, W. Osikowicz, G. Zotti, A. W. D. van der Gon, F. Louwet, M. Fahlman, L. Groenendaal, F. De Schryver, W. R. Salaneck, *J. Polym. Sci., Part B: Polym. Phys.* **2003**, *41*, 2561.

[32] R. Tipnis, S. Vaddiraju, F. Jain, D. J. Burgess, F. Papadimitrakopoulos, *J. Diabetes Sci. Technol.* **2007**, *1*, 193.

[33] P.-J. Chia, S. Sivaramakrishnan, M. Zhou, R.-Q. Png, L.-L. Chua, R. H. Friend, P. K. H. Ho, *Phys. Rev. Lett.* **2009**, *102*, 096602.

[34] F. Günes, H.-J. Shin, C. Biswas, G. H. Han, E. S. Kim, S. J. Chae, J.-Y. Choi, Y. H. Lee, *ACS Nano* **2010**, *4*, 4595.

[35] Z. Liu, J. Li, Z.-H. Sun, G. Tai, S.-P. Lau, F. Yan, *ACS Nano* **2012**, *6*, 810.

[36] J. Ouyang, Q. Xu, C.-W. Chu, Y. Yang, G. Li, J. Shinar, *Polymer* **2004**, *45*, 8443.

[37] S. R. Forrest, *Nature* **2004**, *428*, 911.

[38] F. C. Krebs, *Sol. Energy Mater. Sol. Cells* **2009**, *93*, 394.

[39] A. Stapleton, B. Vaughan, B. Xue, E. Sesa, K. Burke, X. Zhou, G. Bryant, O. Werzer, A. Nelson, A. L. David Kilcoyne, L. Thomsen, E. Wanless, W. Belcher, P. Dastoor, *Sol. Energy Mater. Sol. Cells* **2012**, *102*, 114.

[40] L. Chen, P. Degenaar, D. D. C. Bradley, *Adv. Mater.* **2008**, *20*, 1679.

[41] N. Kim, B. H. Lee, D. Choi, G. Kim, H. Kim, J.-R. Kim, J. Lee, Y. H. Kahng, K. Lee, *Phys. Rev. Lett.* **2012**, *109*, 106405.

[42] T. Takano, H. Masunaga, A. Fujiwara, H. Okuzaki, T. Sasaki, *Macromolecules* **2012**, *45*, 3859.

[43] a) H. Ishii, K. Sugiyama, E. Ito, K. Seki, *Adv. Mater.* **1999**, *11*, 605; b) S. Lacic, O. Inganäs, *J. Appl. Phys.* **2005**, *97*, 124901; c) A. J. Heeger, *Chem. Soc. Rev.* **2010**, *39*, 2354.
[44] a) H. Kang, S. Hong, J. Lee, K. Lee, *Adv. Mater.* **2012**, *24*, 3005; b) Y. Zhou, C. Fuentes-Hernandez, J. Shim, J. Meyer, A. J. Giordano, H. Li, P. Winget, T. Papadopoulos, H. Cheun, J. Kim, M. Fenoll, A. Dindar, W. Haske, E. Najafabadi, T. M. Khan, H. Sojoudi, S. Barlow, S. Graham, J.-L. Brédas, S. R. Marder, A. Kahn, B. Kippelen, *Science* **2012**, *336*, 327.
[45] F. A. Boroumand, A. Hammiche, G. Hill, D. G. Lidzey, *Adv. Mater.* **2004**, *16*, 252.
[46] a) C. Jeong, P. Nair, M. Khan, M. Lundstrom, M. A. Alam, *Nano Lett.* **2011**, *11*, 5020; b) I. N. Kholmanov, C. W. Magnuson, A. E. Aliev, H. Li, B. Zhang, J. W. Suk, L. L. Zhang, E. Peng, S. H. Mousavi, A. B. Khanikaev, R. Piner, G. Shvets, R. S. Ruoff, *Nano Lett.* **2012**, *12*, 5679.
[47] G. Heywang, F. Jonas, *Adv. Mater.* **1992**, *4*, 116.
[48] T. P. Nguyen, S. A. de Vos, *Appl. Surf. Sci.* **2004**, *221*, 330.
[49] a) A. van Dijken, A. Perro, E. A. Meulenkamp, K. Brunner, *Org. Electron.* **2003**, *4*, 131; b) M. Hirade, C. Adachi, *Appl. Phys. Lett.* **2011**, *99*, 153302.
[50] a) S. Lee, G. Jo, S.-J. Kang, G. Wang, M. Choe, W. Park, D.-Y. Kim, Y. H. Kahng, T. Lee, *Adv. Mater.* **2011**, *23*, 100; b) Y. H. Kahng, S. Lee, M. Choe, G. Jo, W. Park, J. Yoon, W.-K. Hong, C. H. Cho, B. H. Lee, T. Lee, *Nanotechnology* **2011**, *22*, 045706.
[51] B. H. Lee, S. H. Park, H. Back, K. Lee, *Adv. Funct. Mater.* **2011**, *21*, 487.
[52] A. Das, S. Pisana, B. Chakraborty, S. Piscanec, S. K. Saha, U. V. Waghmare, K. S. Novoselov, H. R. Krishnamurthy, A. K. Geim, A. C. Ferrari, A. K. Sood, *Nat. Nanotechnol.* **2008**, *3*, 210.
[53] http://www.lasurface.com/database/elementxps.php (accessed: June, 2013).